Minerals **2012**, *2*, 1-x manuscripts; doi:10.3390/min20x000x

OPEN ACCESS

minerals

ISSN 2075-163X

www.mdpi.com/journal/minerals/

Article

Transmission X-ray Microscopy –A New Tool in Clay Mineral Floccules Characterisation

Marek S. Zbik [1,*], Yen-Fang Song [2*], Ray L. Frost[1] and Chun-Chieh Wang [2]

[1] School of Chemistry, Physics and Mechanical Engineering, Science and Engineering Faculty, Queensland University of Technology, 2 George Street, GPO Box 2434, Brisbane Qld 4001, Australia; E-Mail: r.frost@qut.edu.au

[2] National Synchrotron Radiation Research Center, 101 Hsin-Ann Road, Hsinchu Science Park, Hsinchu 30076, Taiwan, R.O.C.; E-Mail: wang@nsrrc.org.tw

* Author to whom correspondence should be addressed; E-Mails: m.zbik@qut.edu.au (M.S.Z.); song@nsrrc.org.tw (Y.F.S.); Tel.: +61-7-3138-2407; Fax: +61-7-3138-1804.

Received: / Accepted: / Published:

Abstract: Effective flocculation and dewatering of mineral processing streams containing clays are microstructure dependent in clay-water systems. Initial clay flocculation is crucial for the design and new methodology for gas exploitation. Microstructural engineering of clay aggregates using covalent cations and Keggin macromolecules have been monitored using the new state of the art Transmission X-ray Microscope (TXM) with 60 nm tomography resolution installed in the Taiwanese synchrotron. The 3-D reconstructions from TXM images show complex aggregation structures in montmorillonite aqueous suspensions after treatment with Na^{+}, Ca^{2+} and Al_{13} Keggin macromolecules. Na-montmorillonite displays elongated and parallel well-orientated, closed voids cellular network 0.5 to 3 μm in diameter. After treatment by covalent cations, the coagulated structure displays much smaller, randomly orientated and openly connected cells 300–600 nm in diameter. The average distances measured between montmorillonite sheets was around 450 nm , which is less than half of the cells dimension measured in Na-montmorillonite. Most dramatic structural changes were observed after treatment by Al_{13} Keggin where aggregates become arranged in compacted domains of 300 nm average diameter composed of thick face to face oriented sheets, which forms elongated and porous plaits-like aggregates with larger intra-aggregate open and connected voids.

Keywords: transmission x-ray microscope; montmorillonite flocculation; montmorillonite gel; clay microstructure

1. Introduction

Montmorillonites are clay minerals commonly found as components in soils from tempered climates. They are ~~are~~ formed as result of weathering of volcanic glass abundant in ash-beds and basic rocks like basalts. These mineral materials are useful for dam bed impregnation to improve water retention properties and as drilling mud to seal the cut, thus preventing fluid loss. They are also popular ~~stabilising~~stabilizing additives in engine oils, cosmetics, pharmaceutical and chemical industries.

The unusual ~~behaviour~~behavior of montmorillonites, the ability to change volume when wetted (swelling) or dried (shrinking), make soil containing montmorillonites very unstable and hazardous for the building industry, due to foundation movement and poor slope stability. These macroscopic properties are dominated by the structural arrangement of its finest fraction. In this work we show ~~utilisation~~utilization of the relatively new technique called transmission X-ray microscopy (TXM) based on the synchrotron photon source. This technique enables, the study in three dimensions, of montmorillonite gel arranged in voluminous cellular structure and it modification by adding Al_{13} Keggin. This is the macro-molecule carrying high positive charge $[Al_{13}(O)_4(OH)_{24}(H_2O)_{12}]^{7+}$ and may cause reduce of negatively charged on the clay particle surface. All these observations were conducted in the natural aqueous environment.

The first experimental confirmation of montmorillonite clay gel structure was obtained with the advent of transmission electron microscopy (TEM) and scanning electron microscopy (SEM). Rosenquist (1) published a micrograph confirming the existence of the “card house” structure. Bowles (2) and O’Brien (3) confirmed the presence of the honeycomb microstructure in wet clay sediments. Grabowska-Olszewska (4) using cryo-SEM investigations published a large amount of microstructural data from 86 studied samples of wet clay rocks combined with compositional and physical properties. Given the size of clay constituents, SEM was found to be the tool of choice used by scientists studying the microstructure of smectitic clays (5, 6). Sample preparation methods available for such investigations, like partial freeze drying, critical point-drying and cryo-fixation, have been found to introduce many artifacts especially when applied to the study of montmorillonite structure. These artifacts result as a consequence of the low thermal conductivity of water and ice, which only allows a slow rate of heat withdrawal from the specimen~~,~~; thus, the size of the gelled montmorillonite sample must be small enough to freeze quickly limiting the inevitable damage associated with the sampling process.

Different microscopy techniques were developed during recent decades. The development of a high resolution transmission X-ray microscope (7, 8, 9) (TXM), has been actively developed since the availability of synchrotron photon sources. In the soft X-ray range (100eV – 1 keV), a zone plate based TXM (10, 11,) has achieved a spatial resolution of 15 nm, which is a big challenge in the hard X-ray region due to difficulties in zone plate manufacturing. In this article we are basing on the microscope constructed in the National Synchrotron Radiation Research Canter (NSRRC) and described by Yin and colleges for the first time in 2006 (12). Attwood (13) also described this method and the ~~principe~~Principe of nanotomography which was used in present work. In this method we combine two

– dimensional images (2D) taken at different incident X-ray angles, allowing internal structures to be discerned with a spatial ~~recolution~~resolution of around 60 nanometers. Clay aggregates we already studied my different X-ray microscopy methods like described in (14) but this particular method using TXM with nanotomography was pioneering in the clay suspension nano-structure investigation by Zbik since the first publication (15).

The big advantage of the TXM tomography is the possibility to observe clay microstructure in a water environment, artifact free and without sample pre-treatment. This method been tested (16) in the study of kaolinite aggregate micro-structure modified by layered double hydroxide addition in the aqueous suspension. This method may be useful in characterization of selected samples in the field of mineral processing for better understanding way modified aggregates changing their structure. In present work synchrotron based TXM nanotomography method is shown in microstructure ~~characterisation~~characterization of modified clay montmorillonite suspensions.

2. Results and Discussion

The Keggin ion exchanged SWy-2 sample along with Na^{+} and Ca^{2+} modified montmorillonite were subjected to X-ray diffraction to ensure complete exchange as shown in Figure 1. Major peak in montmorillonite modified by Na^{+}, Ca^{2+} and Keggin Al_{13}^{7+} ~~kations~~cations, shifts towards larger (*d*) spaces from 11.75 Å, 14.92 Å to 18.92 Å respectively.

Figure 1. XRD pattern from SWy-2 montmorillonite sample modified using Na^{+}, Ca^{2+} and Keggin Al_{13}^{7+} shown significant shift in the major peak from 001 distance between montmorillonite layers. (Theta is in degrees and intensity in count per second).

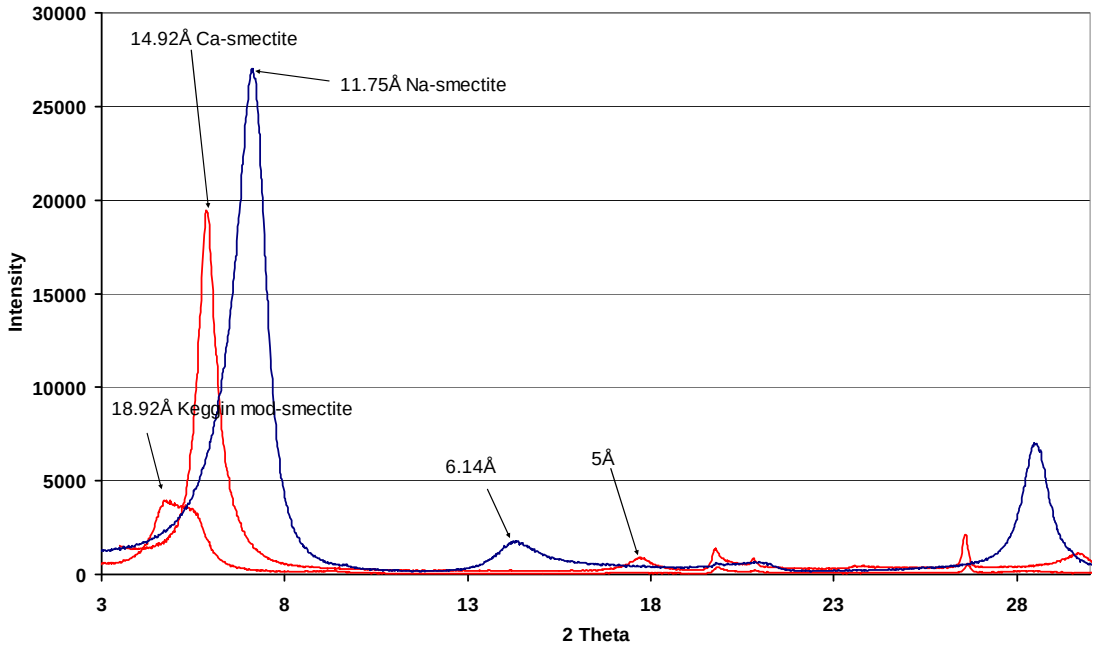

The montmorillonite zeta potential for this montmorillonite as a function of pH as showing in (17) does not display an isoelectric point (iep). For all pH values investigated, the zeta potential of montmorillonite is negative and remains unchanged in magnitude with pH. The pH-independent zeta potential profile results from the dominance of the basal plane or face over the pH-dependent edge surface groups. The basal plane of montmorillonite is negatively charged, due to isomorphoric substitution within the basal surface siloxane layer (18, 19). Because of the week interlayer bonding, montmorillonite naturally disperse in water and stays in suspension or coagulates weakly forming a gel. In the dilute salt solutions SWy-2 montmorillonite individual sheets are highly flexible and interact with each other by a combination of edge-edge (E-E) weak Van der Waals attraction and basal plane (F-F) repulsion building in result an expanded and extremely voluminous cellular network. Earlier works like in M'Ewen and Pratt 1957 (20), predicted that Na-montmorillonite diluted suspension gels in form of the three-dimensional structure, based on a system of cross-linked ribbons. Similar ~~structure are~~structure is presented our TXM 3D anaglyphic micrograph in Figure 2a. In such an extended cellular network flexible montmorillonite sheets encapsulate water within cellular voids

up to 0.5-2 µm in dimension. Geometry of this network can be easily modified by shear, resulting in highly oriented cells, which may evolve. This flocked cellular structure may fill the entire vessel or be fragmented to individual flocks, which differ in size. When structured clay spans all volume I which it is placed, the suspension is gelled; there is no free settling in this system and further compacting may evolve slowly by structural re-arrangement of the entire network (17). The slightest water movement influences shear, which promotes orientation in the entire network as weak electrostatic forces cannot resist. In our view this ribbon-like structure may be resulting from higher E-E Van der Waals attraction as compared with edge to face (E-F) forces. Then as the ribbons flop around, areas of basal surface become attached where the surface charge density is slightly higher. Anaglyphic pictures were obtained from 2D images of different incident angle and were produced using standard Photoshop software. This type of display was chosen to display stereoscopic view of studied structures as the best way to display it in the 2D publication. Micrographs have to be viewed using red and blue glasses.

Figure 2. The high magnification TXM micrographs of 5wt% montmorillonite colloidal gel in water; stereoscopic TXM anaglyphs (**a**) Na saturated at exchangeable position; (**b**) Ca saturated at exchangeable position; (**c**) Al_{13} Keggin treated.

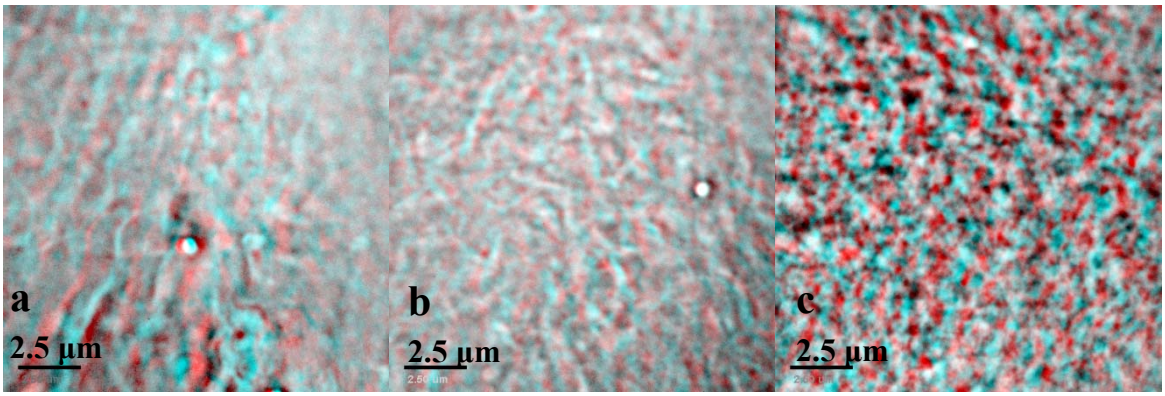

Oriented structure ~~of montmorillonite~~of montmorillonite sheets resemble domains consisted with individual sheets and/or stacked on top of each other and forming laminar elongated cellular network. Such ribbon-like structure can be seen in 3D, TXM tomographic reconstruction which can be studied and measurements were carry out from moving images using the Amira software. Also these image can be displayed in form of anaglyphic micrograph as shown in Fig 2. In micrograph (Fig. 2a), elongated montmorillonite sheets in Na-montmorillonite forms cellular network 0.5 to 2 µm in diameter (average 940 nm). In 3D, TXM anaglyphic micrograph shown in Fig. 2b, Ca-montmorillonite gel cellular structure displays much smaller and mostly randomly oriented cells with dimensions 300-600 nm. The average distances measured between montmorillonite sheets was around 450 nm, which is less than half of the cells dimension measured in Na-montmorillonite.

Most dramatic structural changes were observed after SWy-2 was treated by Al_{13} "Keggin" As can be seen from Fig. 2c, montmorillonite domains become arranged in more compacted network of thicker stacked platelets about 300 nm thick, which are building thick aggregated chains. Studied in water suspension, short-chained aggregates are arranged into parallel orientated elongated, spongy plaits-like ribbons, which are shown in the stereoscopic TXM anaglyphic micrograph Fig 2c. Individual chain aggregates are cross-linked to each other, often with smaller spongy edge to edge (E-

E) platelets assembled in closed loops. Within aggregates, voids are very small and about 30% of total measured porosity belongs to voids of diameter up to 600 nm. Larger channel-like and spherical voids up to 0.5-1.5 µm in diameter are these, which form between plaits-like aggregates. They are lower in number but very important in dewatering because they significantly contribute in flock permeability. Compacted chain aggregates of irregular shape , which assembling in long plates-like are also cross-linked to neighbor similar structural elements by bridges of face to edge orientated thick stack domains as shown in TXM micrograph Fig. 2c which integrating all spongy 3D cellular network. Cells look clear inside and whole structure appears to be ~~stabilised~~stabilized by strength of the chain assembly and reinforced between contacting platelets. Elongated walls of cellular pattern consist with thick (up to 300 nm) aggregates of stairstep-like arranged domains can be observed.

Described differences in the microstructural types probably reflect the difference in the Gibbs energy position and may be explained on the basis of DLVO theory (18). In case of the Keggin modified montmorillonite~~, particles,were~~particles were assembled in low porosity and thick domains as e result of falling into the primary energy minimum on the variation of free energy with particle separation according to DLVO theory. In this case the Van der Waals forces act between FF oriented montmorillonite flakes and aggregates become approach irreversible flocculation.

In our TXM investigations we also used gallium based "Keggin" macromolecule as we assumed that Ga will ~~enchance~~enhance visibility of aggregates as it absorbs more X-ray than aluminium. We found no differences between Al and Ga based Keggin in regard to the better presentation in X-ray micrographs.

Figure 3. The TXM 3D anaglyphic computer reconstruction of 5wt% montmorillonite colloidal gel in water; (**a**) Na saturated at exchangeable position; (**b**) Ca saturated at exchangeable position.

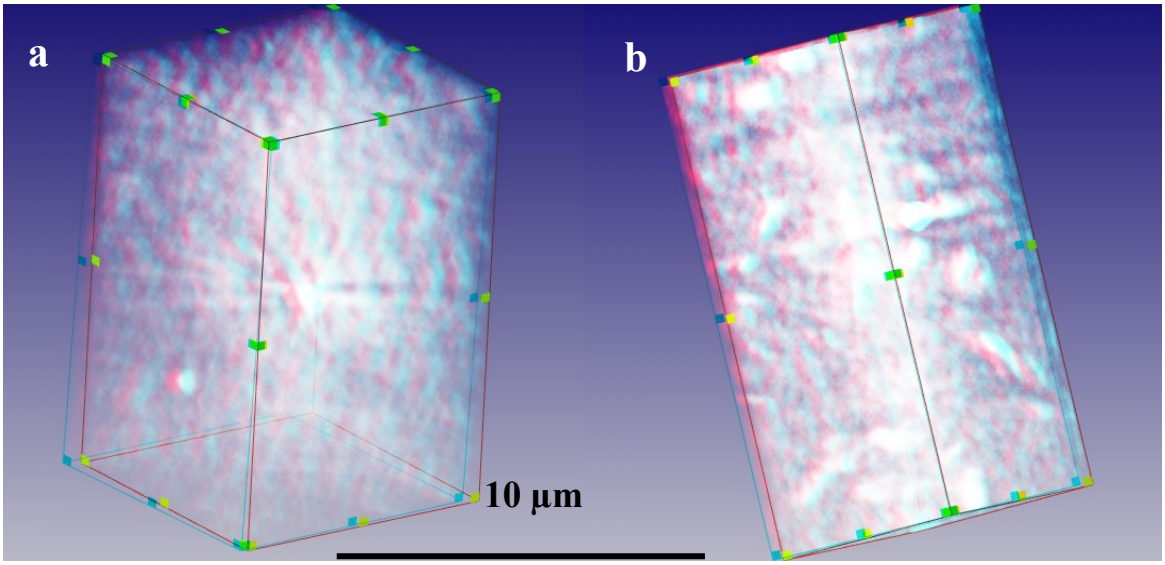

Anaglyphic images shown in Fig. 3. represent three-dimensional (3D) computer reconstructions of Na and Ca-montmorillonite (SWy-2) structures. They are in ~~slighty~~slightly lower resolution than 2D X-ray photographs from which stereoscopic images were assembled in previous Fig. 2. These images

are shown for the better understanding of how the assembly of particles is arranged over the larger volume. These space reconstruction were obtained from 2D pictures of particles observed from different accident angles +70 to -70 degrees (it is possible to observe this gelled suspensions from different angles during investigations). Such angle range was used because of flat microscopy stage available for this investigations. ~~Erliers~~Earlier attempts to use plastic ~~cappilares~~capillaries for 90 degree tomography (15) proven difficult~~icultied~~ using this method. Such a reconstruction reveals the cellular orientation of associated mineral sheets within aqueous suspension as well as observing significant differences in sheet thicknesses between Na and Ca-montmorillonite, observed from different angles.

Similar structural pattern to these observed in high resolution micrographs can be seen in the 2D section taken from the 3D computer reconstructions. Micrographs in sections shown in Fig. 4 demonstrate the basic differences between different sample structural patterns. These images were subjected of image ~~analysing~~analyzing technique called STIMAN and described in details in (6). The **STIMAN** is the **ST**atistical **IM**age **AN**alysing technique designed at Moscow State University and was originally an approach and software for statistically comparison SEM images of different soil ~~tupes~~types. In (6) we utilized it to suspension structural description and in present contribution is used to obtain information about TXM sections. Selected statistical results obtained using STIMAN from selected sections are presented in Fig. 5.

In the Fig. ~~4a ,~~4a, which is cross section of the 3D reconstruction of Na-montmorillonite gel in water show distinctive parallel arrangement of montmorillonite domains, which differ in thickness. Large and closed empty voids in between are the cells observed in high magnification micrograph in Fig. 2a. Water in these large cellular voids looks to be permeable encapsulated.

A much different pattern is shown in Ca-montmorillonite, (Fig. 4b) where denser spherical aggregates are seen and larger empty spaces between these aggregates are filled by water. Porous cellular structure of these aggregates was displayed in TXM micrograph in Fig. 2b. Water in these large irregular inter-aggregate inter-connected voids, can be mobile when within small intra-aggregate closed voids water looks to be permeable encapsulated.

Figure 4. TXM slices of 5wt% montmorillonite in water; (**a**) Na saturated at exchangeable position; (**b**) Ca saturated at exchangeable position; (**c**) Al_{13} Keggin treated. White areas represent particles and black areas belongs to voids.

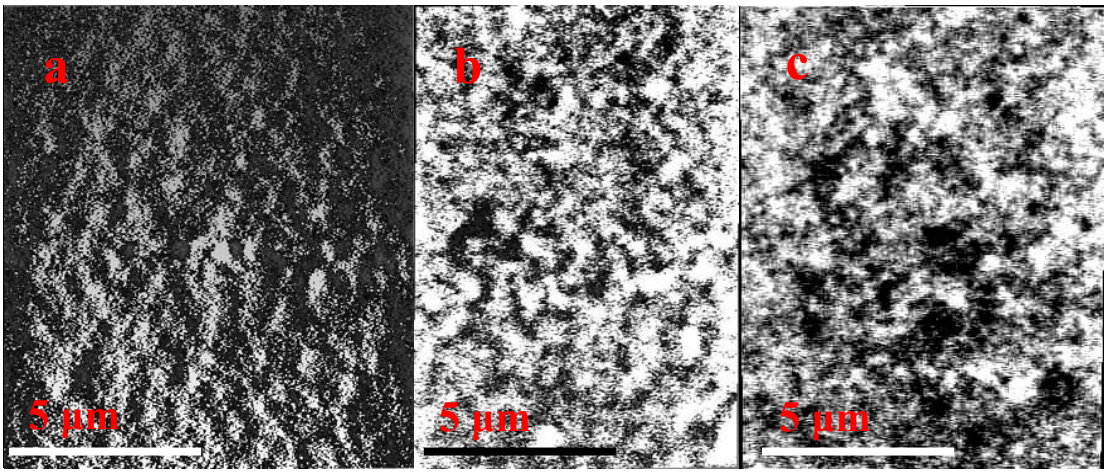

As shown in Al_{13}-SWy-2, Fig. 4c, compact aggregates are arranged in the plaits-like long chains, which are frequently connecting each other by clay assembled bridges. Large voids between aggregates as well as these within aggregates seem to be connected and more regular in shape.

Direct measurements of forces acting between studied Na and Ca-montmorillonites were described in (21) and show a long-range repulsion between the ~~surface~~surfaces of these particles. These long range repulsive forces have been detected from distances over ~1000 nm of the surface separation in case of Na-montmorillonite where in case of Ca-montmorillonite repulsive forces were detected from distances of about ~400 nm. These results are consistent with void sizes observed in the TXM images.

Selected statistical results obtained from ~~analysing~~analyzing cross sections of computer reconstruction images as shown in Fig. 4 are presented in the form of diagrams (Fig. 5). Aggregates and voids were studied. Diagrams in Fig. 5a show total particle distribution across their diameter. These graphs show smallest particles build aggregates in the Na-Swy-2 water gel, where mostly representative were particles of 450 nm in diameter and these particles were assembled into larger elongated aggregates. Most particles were below 1 μm in the equivalent diameter which is diameter of ideal, spherical particle that settling in the same rate in the aqueous environment. Ca and Al_{13}-montmorillonites display much larger aggregates where most of them are between 1 and 3 μm in the equivalent diameter.

Results of voids distribution over equivalent diameters are shown in Fig. 5b. Results show very broad voids distribution over smaller diameters ranging from 200 nm up to 1 μm. The majority of voids in Na-montmorillonite are represented by this range of diameters range and only 35% voids are 2.5-3 μm in diameters. These larger voids are perhaps these cellular elongated voids observed in TXM micrographs. The graphs did not show us if these voids are connected. Consequently, majority of voids in Ca and Al_{13}-montmorillonites groups within 1-3 μm in diameter. In Ca-montmorillonite voids frequency distribution steady increase over the diameter range when in the Al_{13}-montmorillonite distribution increase sharply in the range of diameters between 1.2-2.5 μm.

Permeability of studied systems was shown in Fig. 5c as the filtration coefficient distribution across voids of different diameters. The smallest value of permeability was obtained for Na-montmorillonite water system. The maximum seen in larger voids diameter range do not make this structure permeable because these voids are more likely are cellular and closed. A wider range of larger filtration coefficients were obtained for Ca and Al_{13}-montmorillonite and because larger voids responsible for this larger permeability are open it is more likely to dewater these structural systems more easily.

The form index of studied voids is shown in Fig. 5d. This parameter displays evolution from mostly elongated void forms in Na-montmorillonite structure, to a more equal distribution in Ca-montmorillonite structure and to mostly regular voids within Al_{13}-montmorillonite structural type.

Figure 5. Results of the STIMAN statistical results drawn from TXM micrographs, (**a**) frequency of aggregates distribution according to their total area for Na^+, Ca^{2+} cationic form and Al_{13} treated clay respectively. In the Y axis units is the probability density; (**b**) frequency of voids distribution accordingly to their total area voids for Na^+, Ca^{2+} cationic form and Al_{13} treated clay respectively. In the Y axis units is the probability density; (**c**) voids contribution in filtration for Na^+ & Ca^{2+} cationic and Al_{13} treated clay respectively.

In the Y axis units is the filtration coefficient in Darcy (D); (d) The voids form index for Na^{+} & Ca^{2+} cationic and Al_{13} treated clay respectively.

(a)

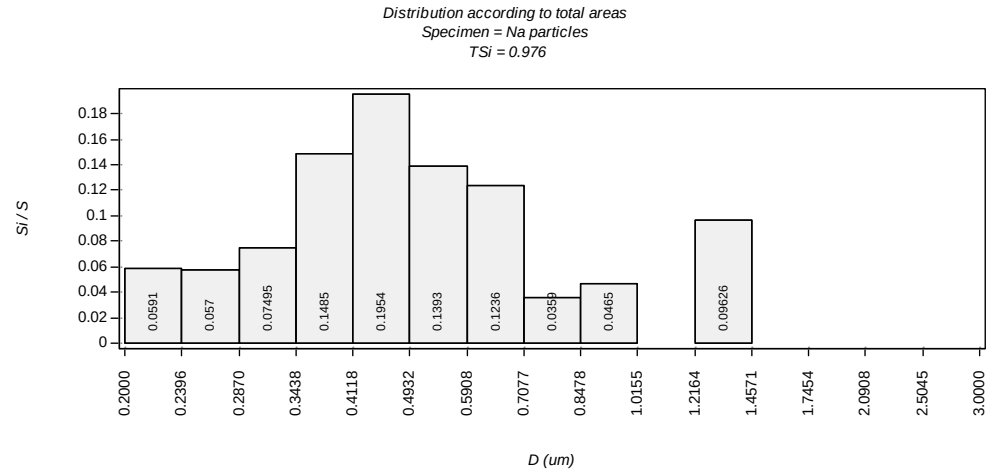

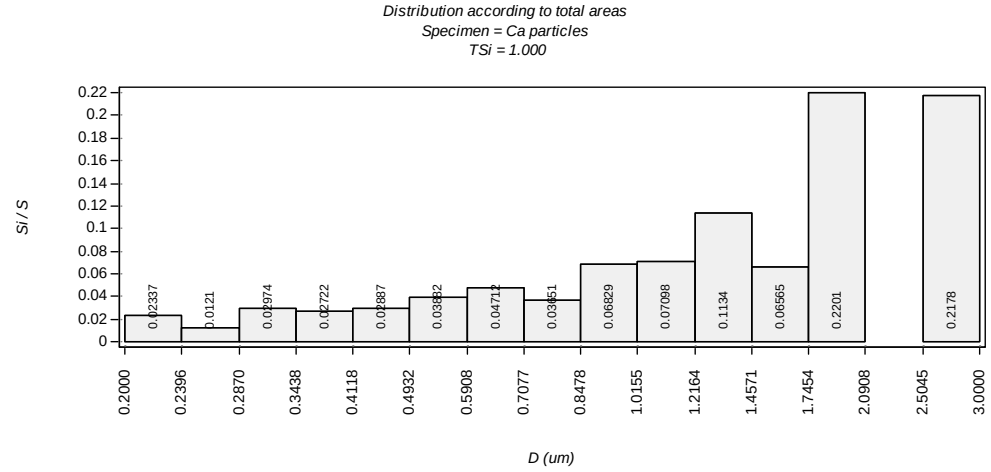

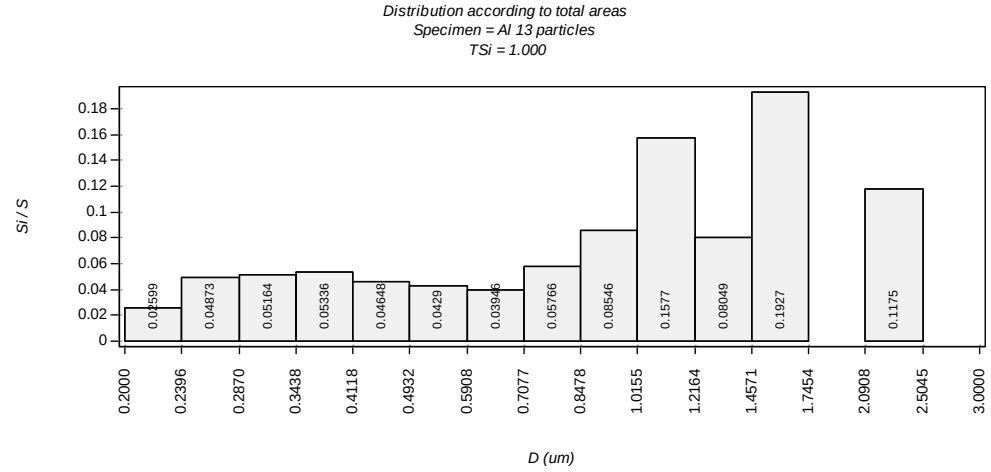

(b)

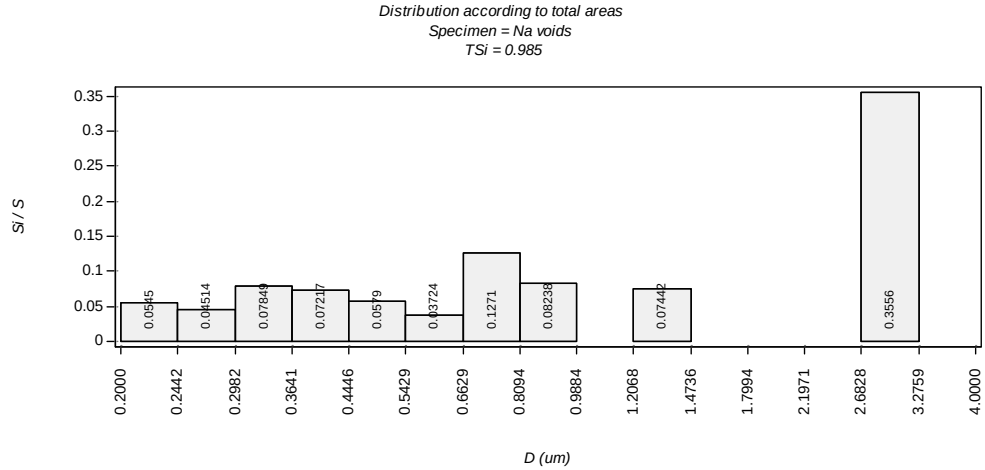
Distribution according to total areas
Specimen = Na voids
TSi = 0.985
Si / S
D (um)
0.0545
0.04514
0.07849
0.07217
0.0579
0.03724
0.1271
0.08238
0.07442
0.3556
0.2000
0.2442
0.2982
0.3641
0.4446
0.5429
0.6629
0.8094
0.9884
1.2068
1.4736
1.7994
2.1971
2.6828
3.2759
4.0000

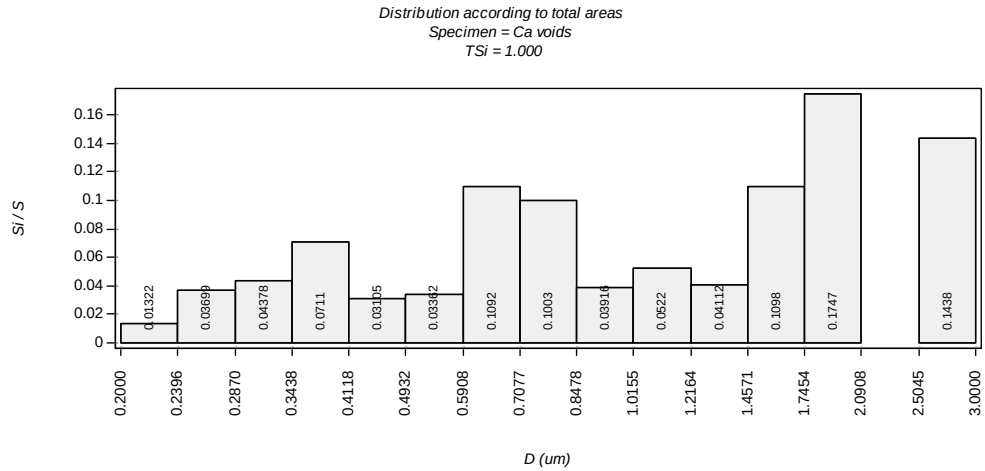
Distribution according to total areas
Specimen = Ca voids
TSi = 1.000
Si / S
D (um)
0.01322
0.03699
0.04378
0.0711
0.03105
0.03342
0.1092
0.1003
0.03916
0.0522
0.04112
0.1098
0.1747
0.1438
0.2000
0.2396
0.2870
0.3438
0.4118
0.4932
0.5908
0.7077
0.8478
1.0155
1.2164
1.4571
1.7454
2.0908
2.5045
3.0000

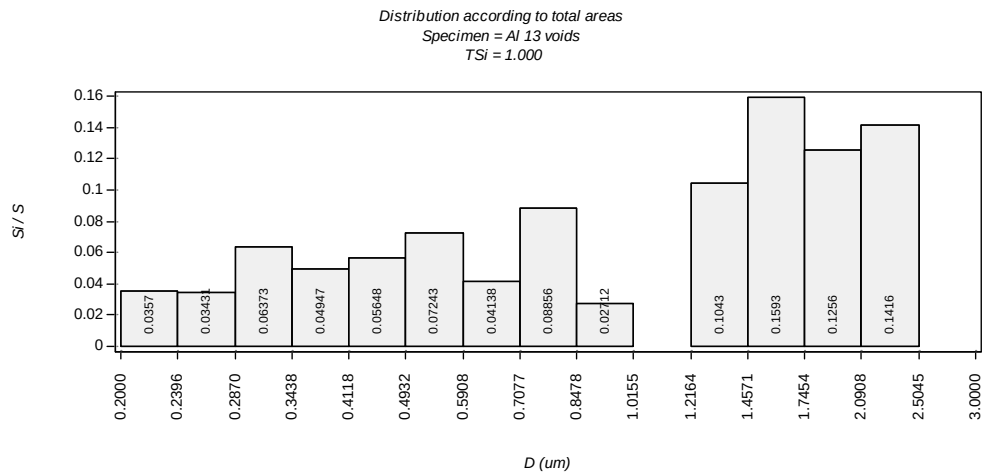
Distribution according to total areas
Specimen = Al 13 voids
TSi = 1.000
Si / S
D (um)
0.0357
0.03431
0.06373
0.04947
0.05648
0.07243
0.04138
0.08856
0.02712
0.1043
0.1593
0.1256
0.1416
0.2000
0.2396
0.2870
0.3438
0.4118
0.4932
0.5908
0.7077
0.8478
1.0155
1.2164
1.4571
1.7454
2.0908
2.5045
3.0000

(c)

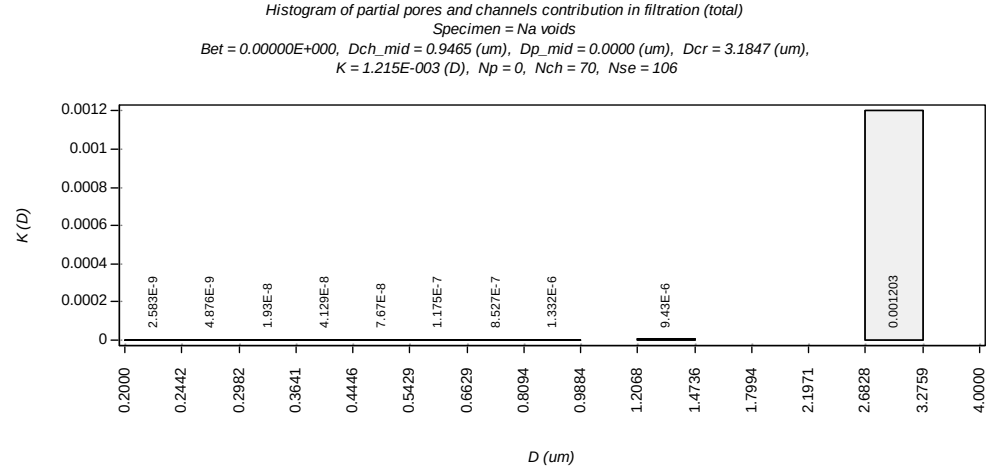
Histogram of partial pores and channels contribution in filtration (total)
Specimen = Na voids
Bet = 0.00000E+000, Dch_mid = 0.9465 (um), Dp_mid = 0.0000 (um), Dcr = 3.1847 (um),
K = 1.215E-003 (D), Np = 0, Nch = 70, Nse = 106
K (D)
0.0012
0.001
0.0008
0.0006
0.0004
0.0002
0
2.583E-9
4.876E-9
1.93E-8
4.129E-8
7.67E-8
1.175E-7
8.527E-7
1.332E-6
9.43E-6
0.001203
0.2000
0.2442
0.2982
0.3641
0.4446
0.5429
0.6629
0.8094
0.9884
1.2068
1.4736
1.7994
2.1971
2.6828
3.2759
4.0000
D (um)

1

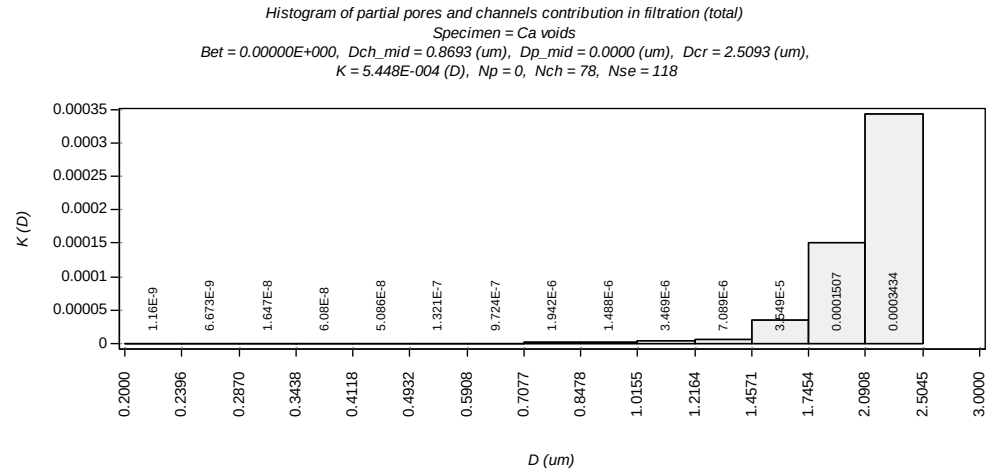
Histogram of partial pores and channels contribution in filtration (total)
Specimen = Ca voids
Bet = 0.00000E+000, Dch_mid = 0.8693 (um), Dp_mid = 0.0000 (um), Dcr = 2.5093 (um),
K = 5.448E-004 (D), Np = 0, Nch = 78, Nse = 118
K (D)
0.00035
0.0003
0.00025
0.0002
0.00015
0.0001
0.00005
0
1.16E-9
6.673E-9
1.647E-8
6.08E-8
5.086E-8
1.321E-7
9.724E-7
1.942E-6
1.488E-6
3.469E-6
7.089E-6
3.549E-5
0.0001507
0.0003434
0.2000
0.2396
0.2870
0.3438
0.4118
0.4932
0.5908
0.7077
0.8478
1.0155
1.2164
1.4571
1.7454
2.0908
2.5045
3.0000
D (um)

2

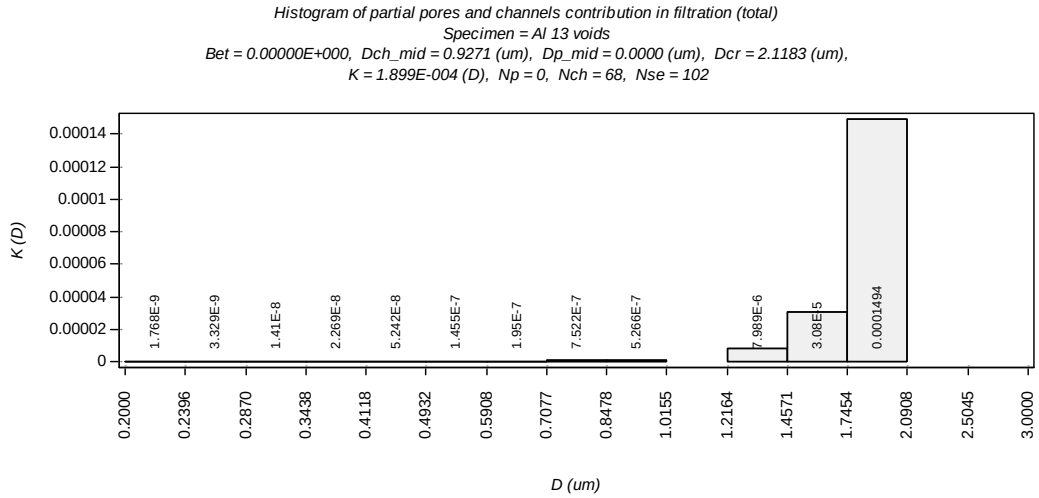
Histogram of partial pores and channels contribution in filtration (total)
Specimen = Al 13 voids
Bet = 0.00000E+000, Dch_mid = 0.9271 (um), Dp_mid = 0.0000 (um), Dcr = 2.1183 (um),
K = 1.899E-004 (D), Np = 0, Nch = 68, Nse = 102
K (D)
0.00014
0.00012
0.0001
0.00008
0.00006
0.00004
0.00002
0
1.768E-9
3.329E-9
1.41E-8
2.269E-8
5.242E-8
1.455E-7
1.95E-7
7.522E-7
5.266E-7
7.989E-6
3.08E-5
0.0001494
0.2000
0.2396
0.2870
0.3438
0.4118
0.4932
0.5908
0.7077
0.8478
1.0155
1.2164
1.4571
1.7454
2.0908
2.5045
3.0000
D (um)

3

4

(d)

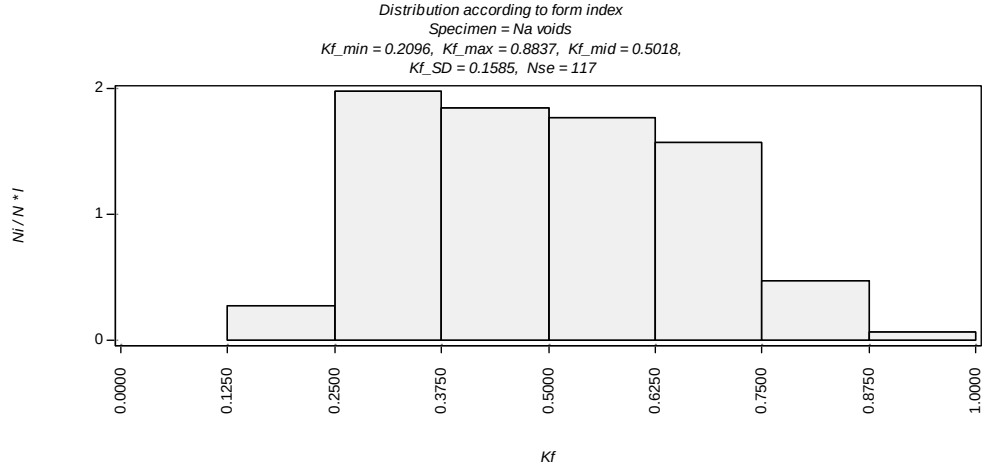

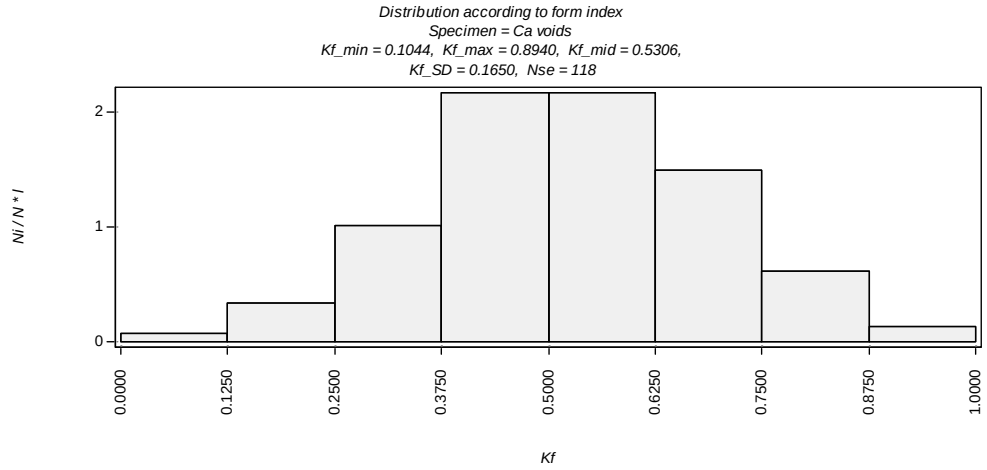

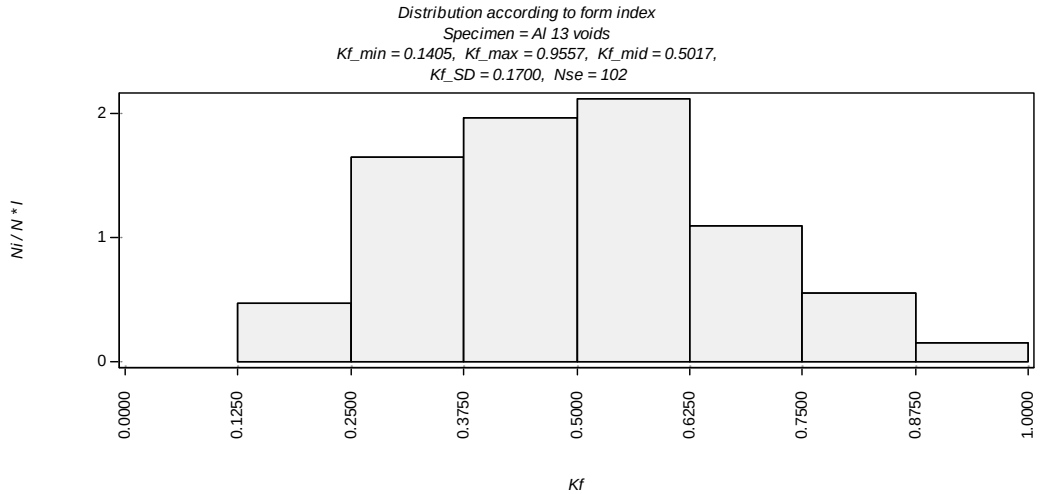

3. Experimental Section

The transmission X-ray microscopy (TXM) with 60 nm tomographic resolution has been installed at beamline BL01B of NSRRC in Taiwan with a superconducting wavelength shifter source, , which provides a photon flux of 5 x 10^{12} photons/s/0.1 % bw in the energy range 5-20 keV. X-rays generated by a wavelength shifter are primarily focused at the charge coupled detector by a toroidal focusing mirror with focal ratio nearly 1:1. A double crystal monochromator exploiting a pair of Ge (111) crystals selects X-rays of energy 8-11 keV. After the focusing mirror and double crystal monochromator, the X-rays are further shaped by a capillary condenser. Its entrance aperture is about 300 μm, with an end opening of about 200 μm and is 15 cm long. This capillary condenser gives a reflection angle of 0.5 mrad with respect to the propagation direction. The condenser intercepts the impinging X-rays and further focuses them onto the sample with ~~focussing~~focusing efficiency is as high as 90% of the total focus, due to the internal totally reflecting nature inside the capillary. The zone-plate is a circular diffraction grating consisting of alternating opaque and transparent concentric zones. In the microscope, the zone-plate is being used as an objective lens magnifying the images 44× and 132× for the first order and third order diffraction mode, respectively. Conjugated with a 20× downstream optical magnification, the microscope provides total magnification of 880× and 2640× for first order and third diffraction order mode, respectively.

This technique, however has some limitations (15), which were overcome and the method been recently tested in the study of different clay minerals like kaolinite (16, 22) and montmorillonite (21) clay samples. This method shows progress in discrete structure imaging of the clay-water aggregates and in ~~visualisation~~visualization of structural modifications. These modifications may have significant impact on the macroscopical ~~behaviour~~behavior of resulting, subject to modification, clay materials.

The montmorillonite used in this study was the well known Na-montmorillonite from Wyoming (U.S.A.) obtained from Clay Mineral Repository. This sample (SWy-2) has been well described (23) and two samples were prepared from this original clay. First the colloidal fraction was separated by centrifugation and secondly all cations in exchangeable positions were ion exchanged with sodium Na^{+} and calcium Ca^{2+} ions by saturating original montmorillonite sample in chlorine 1 N salt solution over 24 hours and ~~dialised~~dialyzed it until no reaction on Cl was detected.. Measurements were performed in deionised water of unknown ionic strength. Note that it is difficult to control Debye length in "water" because there is always some low level, 0.01 mM or less, of background electrolyte (including ions from the self-dissociation of water) that is hard to quantify or control. The most important difference in the bonding between Ca- and Na-montmorillonite sheets is that the spacing between most of the former (Ca- montmorillonite) is restricted to 0.95 nm, whereas the spacing of the latter (Na-montmorillonite) can be unlimited (15).

Preparation of intercalated SWy-2 ~~montmorillinite~~montmorillonite and solutions of aluminium and gallium 13 Keggin ions where prepared by a method similar to (24). Solutions of sodium hydroxide (0.10M), aluminium nitrate (0.05M) and gallium nitrate (0.05M) were prepared in filtered water (18.2MΩ). A peristaltic pump was used to add the hydroxide solution (0.125% of the solution per minute) to a solution of the metal nitrate in a molar ratio of 2:1 (hydroxide: metal). The cluster cation $(Al_{13}O_4(OH)_{24}(H_2O)_{12})^{7+}$ has the Keggin structure with a tetrahedral Al atom in the centre of the cluster coordinated to 4 oxygen atoms. This ion is generally called the Al_{13} ion. A Ga_{13} analogue is known and also was used in our experiments to investigate whether Ga atoms have greater absorption in contrast to the Al atoms.

The resultant Keggin ion solution was allowed to age over night before use. To an aliquot of the Keggin ion solution, the sodium exchanged SWy-2 was added in an amount, which ensured the Keggin ion remained four times the Cation Exchange Capacity (CEC). The clay in Keggin ion solution was mixed overnight using a magnetic stirrer before collection, washing and drying via vacuum filtration. Before redispersing for structural examination, the sample was grounded and mixed with deionised water.

Suspension sample (100 ml) were transported to Taiwanese synchrotron where fraction of a droplet was placed into the square steel frame and secured from both sides by Kapton tape. Suspension layer within the microscopy stage was >100 μm. 3D tomography was reconstructed based on 141 sequential images taken in first order diffraction mode with azimuth angle rotating.

4. Conclusions

Our TXM investigations reveal swollen cellular structure in aqueous montmorillonite gel with void diameters on the ~~micrometre~~micrometer scale, which is consistent with previously published AFM force measurements (21). Na-montmorillonite diluted suspension gels in form of the three-dimensional structure, based on a system of cross-linked ribbons. These ribbons like aggregates form highly orientated, spacious cellular network where cells up to 1-2 μm in diameter. They form~~ing~~ laminar elongated cellular liquid crystal-like micelles. Voids in this structure seem to be closed and not to be connected and system became mostly impermeable.

This network encapsulates water within impregnable elongated cellular structure. A different, coagulated aggregate type of micro-structure has been observed in Ca-montmorillonite with cells having a diameter of ~0.4 μm and shorter within aggregates and 1-3 μm voids between aggregates. Thicker and more rigid structural network elements are multi-sheet assembly, which are mostly randomly orientated and were more resistant to shear forces. All voids look more open than in case of Na-montmorillonite and connected with ~~neighbours voids~~neighbors voids. The inter-aggregate channels are elongated and seem to be connected with more regular in shape intra-aggregate voids.

The Keggin modified montmorillonite displays significantly different microstructural type where montmorillonite flakes stacked into Face-to-Face (FF) and Edge-to Face (EF) orientated particles build denser aggregates, which assembled long spongy plaits-like super-aggregates. These aggregates are bridged to other similar aggregates in random direction. Large and connected voids system generates larger permeability of such a structure allowing better sediments dewatering.

This novel preparative method using synchrotron based TXM nanotomorgaphy technique can be use in the field of mineral processing as a tool to better understand micro-structural changes during operations. Because this method is involves more time and special equipment which is not presently available in Australia, cannot be commonly implemented. However a lot of industrial institutions having academic partner for their linkage project and in such instances it can be very useful to moving forward our ~~frontiere~~frontier of knowledge in the field of mineral processing. It is also very likely that modernization of X-ray microscopy techniques brings soon techniques much cheaper and suitable for ~~rutine~~routine structural monitoring. Such a monitoring can directing technological processes to ~~acheve~~achieve desire material properties which are determined almost exclusively by the microstructural design.

The TXM technique allows us to monitor aggregate structure within natural water environments and give more accurate description of processes. This technique is in a state of evolution and in the near future will be most valuable for monitoring in mineral processing.

Acknowledgments

This work was supported by the Australian Synchrotron Research Program (ASRP).
Authors thanks to anonymous reviewers for very helpful contribution.

References

1. Rosenquist, J.T. Physico-Chemical Properties of Soil: Soil – Water Systems. *J. Soil Mech. And Found. Division, Proc. ASCE* Sm 2, **1959**, 85, 31-53.
2. Bowles, F.A. Microstructure of Sediments: Investigation with Ultrathin Sections. *Science*, **1968**, 159, 1236-12371.
3. O'Brien, N.R. Fabric of Kaolinite and Illite Floccules. *Clays and Clay Minerals*, **1971**, 19, 353-359.
4. Grabowska-Olszewska, B.; Osipov, V.; Sokolov, Vi. In *Atlas of the Microstructure of Clay Soils*: PWN, Warszawa, Poland, 1984; pp. 49-52.
5. Smart, P. Tovey, N.K. In *Electron Microscopy of Soils and Sediments: Techniques.* Clarendon Press, Oxford, UK, 1982, pp. 84-132.
6. Smart, R.St.C.; Żbik, M.; Morris, G.E. STIMAN observation of aggregate structure in clay flocculation, in (J.S. Laskowski Edt.) *43rd Annual Conference of Metallurgists of CIM*. **2004**, 215-228.
7. Schneider, G. Cryo X-ray microscopy with high spatial resolution in amplitude and phase contrast. Ultramicroscopy **1998**, 75, 85 – 104.
8. Neuhäusler, U.; Schneider, G.;Ludwig, W.; Meyer, M.A.;Zschech E and Hambach D. X-ray microscopy in Zernike phase contrast mode at 4 keV photon energy with 60 nm resolution. *J. Phys. D: Appl. Phys.* **2003**, 36, A79–A82
9. Meyer-Ilse, W.;Medecki, H.; Brown, J.T.;Heck, J.; Anderson, E.; Magowan, C.; Stead, A.; Ford, T.;Balhorn, R.; Petersen, C. and Attwood, D.T. *X-ray Microscopy and Spectromicroscopy.* **1997**, Springer, Berlin,
10. Di Fabrizio E.; Romanato F.; Gentili, M.; Cabrini, S.; Kaulich, B.; Susini, J. and Barrett, R. High-efficiency multilevel zone plates for keV X-rays. *Nature*, **1999** 401, 895 – 898.
11. Lai, B.; Yun, W.B.; Legnini, D.; Xiao, Y.; Chrzas, J. and Vidcaro, P.J. Hard x - ray phase zone plate fabricated by lithographic techniques. *Appl. Phys. Lett.* **1992**, 61, 1877 – 1879.

12. Yin, G-C.; Tang, M-T.; Song, Y-F.; Chen, F-R.; Liang, K. S. ; Duewer, F.W. ; Yun, W ; Ko, C-H.; and Shieh, H-P. D. Energy-tunable transmission x-ray microscope for differential contrast imaging with near 60 nm resolution tomography. *Appl. Phys. Lett*. **2006**, 88, 241115 - 241115-3
13. Attwood, D. Nanotomography comes of age. *Nature*, 2006, 442, 642-643.
14. Niemeyer, J.; Thieme, J.; Guttmann, P.; Wilhein, T.; Rudolph D. and Schmahl G. Direct imaging of aggregates in aqueous clay-suspensions by x-ray microscopy. *Progress in Colloid and Polymer Science* **1994**, 95, 139 – 142.
15. Zbik, M.S.; Frost, R.L.; Song, Y-F. Advantages and limitations of the synchrotron based transmission X-ray microscopy in the study of the clay aggregate structure in aqueous suspensions. *J Coll. Int. Sci.* **2008**, 319, 169-174.
16. Zbik, M.S.; Frost, R.L.; Song, Y-F.; Chen, Y.-M.; Chen, J.-H. Transmission X-ray Microscopy Reveals the Clay Aggregate Discrete Structure in Aqueous Environment, *Journal of Colloid and Interface Science*, 2008, **319**, 457-461.
17. Morris, G.E.; Żbik, M.S. Smectite suspension structural behaviour, *Int. J. Min. Proc*. **2009**, **93**, 20-25.
18. Van Olphen, H. In *An Introduction to Clay Colloid Chemistry*. Wiley, New York, 1977; pp. 58-65.
19. Lagaly, G.; Ziesmer, S. Colloid chemistry of clay minerals: the coagulation of montmorillonite dispersions. *Adv. Colloid Interface Sci.* **2003**, 100–102.
20. M'ewen, M.B. and Pratt, M.I. The Gelation of Montmorillonite. *Trans. Faraday Soc.* **1957**, 53, 535 – 547.
21. Zbik, M.S.; Martens, W.; Frost, R. L.; Song, Y-F.; Chen, Yi-M.; Chen, J-H. Transmission X-ray Microscopy (TXM) reveals nano-structure of smectite gel. *Langmuir*, **2008**, 24, 8954-8958.
22. Zbik, M.S.; Frost, R.L.; Song, Y-F.; Chen, Y.-M.; Chen, J.-H. Transmission X-ray Microscopy Reveals the Clay Aggregate Discrete Structure in Aqueous Environment, *J. Coll. Int. Sci.* **2008**, 319, 457-46.
23. Van Olphen, H.; Fripiat, J.J. In *Data handbook for clay materials and other non-metallic minerals.* Pergamon Press. Oxford; New York. 1979, 183.
24. Aouad, A.; Mandalia, T.; Bergaya, F. A novel method of Al-pillared montmorillonite preparation for potential industrial up-scaling. Appl. Clay Sci. **2005**, 28, 175– 182.